

1 A multi-model ensemble of baseline and process-based models improves the predictive
2 skill of near-term lake forecasts

3 Freya Olsson^{1*}, Tadhg Moore^{1,2}, Cayelan C. Carey¹, Adrienne Breef-Pilz¹, R. Quinn Thomas^{1,3}

4 Freya Olsson: 0000-0002-0483-4489, freyao@vt.edu

5 Tadhg Moore: 0000-0002-3834-8868, tadhgm@vt.edu; tadhg.moore6@gmail.com

6 Cayelan C. Carey: 0000-0001-8835-4476, cayelan@vt.edu

7 Adrienne Breef-Pilz: 0000-0002-6759-0063, abreefpilz@vt.edu

8 R. Quinn Thomas: 0000-0003-1282-7825, rqthomas@vt.edu

9 ¹Department of Biological Sciences, Virginia Tech, Blacksburg, Virginia, USA 24061

10 ²Independent researcher

11 ³Department of Forest Resources and Environmental Conservation, Virginia Tech, Blacksburg,
12 Virginia, USA 24061

13 *Corresponding author (freyao@vt.edu)

14 **Keywords**

15 forecasting; multi-model ensemble; water temperature; process-based models; baseline models

16 **Key points** (140 characters)

- 17
- 18 • Aggregated lake temperature forecast skill was higher for multi-model ensemble
19 forecasts than individual model forecasts
 - 20 • Including baseline empirical models (climatology, persistence) with process models
21 improved multi-model ensemble forecast performance
 - 22 • Multi-model ensemble forecasts improved forecast skill by ‘hedging’, as no individual
23 model performed best at all horizons or depths

23 **Abstract**

24 Water temperature forecasting in lakes and reservoirs is a valuable tool to manage crucial
25 freshwater resources in a changing and more variable climate, but previous efforts have yet to
26 identify an optimal modelling approach. Here, we demonstrate the first multi-model ensemble
27 (MME) reservoir water temperature forecast, a forecasting method that combines individual
28 model strengths in a single forecasting framework. We developed two MMEs: a three-model
29 process-based MME and a five-model MME that includes process-based and empirical models
30 to forecast water temperature profiles at a temperate drinking water reservoir. Our results
31 showed that the five-model MME improved forecast performance by 8-30% relative to individual

32 models and the process-based MME, as quantified using an aggregated probabilistic skill score.
33 This increase in performance was due to large improvements in forecast bias in the five-model
34 MME, despite increases in forecast uncertainty. High correlation among the process-based
35 models resulted in little improvement in forecast performance in the process-based MME
36 relative to the individual process-based models. The utility of MMEs is highlighted by two
37 results: 1) no individual model performed best at every depth and horizon (days in the future),
38 and 2) MMEs avoided poor performances by rarely producing the worst forecast for any single
39 forecasted period (<6% of the worst ranked forecasts over time). This work presents an
40 example of how existing models can be combined to improve water temperature forecasting in
41 lakes and reservoirs and discusses the value of utilising MMEs, rather than individual models, in
42 operational forecasts.

43 **1 Introduction**

44 In the face of increased ecosystem variability, researchers are developing new methods for
45 forecasting freshwater quality and quantity (Lofton et al., 2023). Here, we define a forecast as a
46 prediction of a future state of a variable with quantified uncertainty (Lewis et al., 2022).
47 Forecasts of freshwater variables have considerable potential for improving management and
48 guiding ecosystem service provision as environmental conditions increasingly exceed the
49 historical envelope due to climate and land use change (Bradford et al., 2020; Dietze et al.,
50 2018; IPCC, 2023). Despite the urgent need for freshwater forecasts, however, the optimal
51 modelling approach for developing forecasts remains unresolved across different spatial and
52 temporal scales. One promising forecasting approach that has emerged from other disciplines is
53 multi-model ensembles (MMEs), in which more than one model is used to simultaneously
54 forecast the same variable into the future (Chandler, 2013; Clark et al., 2022; Humphries et al.,
55 2018; Kirtman et al., 2014; Long et al., 2021; Velázquez et al., 2011). To date, MMEs have not
56 been applied to freshwater forecasting (reviewed by Lofton et al., 2023), motivating the need to
57 understand how an MME forecast performs relative to individual models, as well as how the
58 structure of the different models in the MME influences forecast performance.

59 Water temperature forecasting in lakes and reservoirs is an ideal application for testing the
60 performance of MMEs. First, water temperature forecasts can be useful for the management of
61 inland waters (Lofton et al., 2023). For example, water temperature forecasts are used to
62 optimise downstream water release from reservoirs (Huang et al., 2011; Jackson-Blake et al.,

63 2022; Weber et al., 2017; Zwart et al., 2023), guide water quality management related to lake
64 mixing events (Carey, Woelmer, et al., 2022; Thomas et al., 2020), as well as underpin the
65 development of other water quality and ecological forecasts (Huang et al., 2011; Page et al.,
66 2018; Weber et al., 2017), given the importance of water temperature for determining
67 metabolism, water chemistry, and biological growth (Carey et al., 2012; Kraemer et al., 2017;
68 Yvon-Durocher et al., 2015). Second, a wide range of models have been developed to predict
69 lake and reservoir water temperatures, thereby providing an excellent opportunity for examining
70 the sensitivity of an MME's performance to the identity and structure of multiple component
71 models.

72 To date, process-based models (Baracchini et al., 2020; Clayner et al., 2023; Mercado-Bettín et
73 al., 2021; Thomas et al., 2020), machine learning and data-driven models (Read et al., 2019;
74 Zhu et al., 2020; Zwart et al., 2023), as well as a range of "hybrid" approaches (e.g. Graf et al.,
75 2019; Zhu et al., 2020) have been used to forecast near-term dynamics (days to seasons
76 ahead) in lake and reservoir water temperatures, with varying levels of performance (reviewed
77 by Lofton et al., 2023). Of these modelling approaches, process-based models (hereafter,
78 process models) have shown substantial promise, especially in near-term forecast horizons
79 (Baracchini et al., 2020; Carey, Woelmer, et al., 2022; Mercado-Bettín et al., 2021; Thomas et
80 al., 2020), with a performance of 0.4 - 1.4 °C RMSE (root mean square error) for reservoir water
81 temperature forecasted 1-16 days-ahead (Thomas et al., 2020). However, the skill of these
82 models is often limited by the skill of other forecasts (e.g., weather and inflow discharge)
83 needed as model driver data (Mercado-Bettín et al., 2021; Thomas et al., 2020). Moreover,
84 process models also often demonstrate substantial differences in skill among forecasted sites
85 (Thomas et al., 2023) and depths (Thomas et al., 2020), as well as at different times of year
86 (e.g., in thermally-stratified vs mixed conditions; Thomas et al., 2020; Wander et al., 2023).

87 Despite their simplicity, simple empirical models such as persistence and climatology (historical
88 day-of-year mean and variance) models can also provide useful forecasts (Ward et al., 2014).
89 Often used as null models to test the skill of emerging forecasting approaches (Lofton et al.,
90 2023; Pappenberger et al., 2015), these simple baseline models include information on current
91 conditions and seasonal trends that influence lake temperature dynamics. For example, a
92 persistence model can be useful for forecasting dynamics in systems with high inertia that
93 exhibit small changes across the forecast horizon (i.e., time into the future; Ward et al., 2014),
94 which is common in lakes and reservoirs that exhibit seasonal thermal stratification. Additionally,

95 climatology forecasts exhibit high performance at longer horizons (e.g., months to years), for
96 which repeatable seasonal cycles dominate the dynamics (Pappenberger et al., 2015).

97 Multi-model ensembles (MMEs) that integrate both process models and these simple baseline
98 models may be particularly effective for forecasting lake and reservoir water temperatures. This
99 type of MME may be able to overcome the limitations of individual process and baseline models
100 that are unable to consistently forecast all environmental conditions with high accuracy across
101 space (i.e., multiple depths in a lake), time (i.e., different seasons within a year), and forecast
102 horizons. Implementation in other disciplines has overwhelmingly found that MMEs often
103 produce more skillful forecasts, on average, than individual model forecasts (Atiya, 2020; Clark
104 et al., 2022; Humphries et al., 2018; Velázquez et al., 2011). Using MMEs also leads to greater
105 diversity in forecast predictions, potentially increasing decision-making success (Boettiger,
106 2022). Although predictions from individual models can outperform the aggregated prediction
107 from the MME locally, at a specific depth, time, or horizon (Abrahart & See, 2002; Atiya, 2020),
108 it is often not known *a priori* which forecast model will be best at any given future timestep,
109 especially for forecasts of sites with substantial spatial and temporal heterogeneity. MMEs are
110 ideally suited for these situations, because they integrate information from different model
111 structures into a single forecast, enabling the forecaster to ‘hedge’ (i.e., minimise risk of
112 incorrect forecasts by assigning non-zero probability to a wide range of possible outcomes) and
113 provide a more comprehensive and accurate representation of the potential forecasted
114 outcomes than individual models (Abrahart & See, 2002; Atiya, 2020). MMEs have been
115 successfully applied to a diverse range of ecological and environmental forecasting applications,
116 including ticks (Clark et al., 2022), sea level (Long et al., 2021), penguins (Humphries et al.,
117 2018), and river flow (Abrahart & See, 2002; Velázquez et al., 2011), suggesting that their
118 application for forecasting freshwater ecosystems has promise.

119 To the best of our knowledge, no one has applied an MME approach to forecasting lake and
120 reservoir temperatures with specified uncertainty. While MMEs for water temperatures have
121 been applied to long-term projections (Almeida et al., 2022; Feldbauer et al., 2022; La Fuente et
122 al., 2022; Wynne et al., 2023), or as model inter-comparisons (Golub et al., 2022), the utility of
123 MMEs for real-time water temperature forecasting remains unknown. This gap may exist
124 because ensemble near-term forecasts have, to date, focused on using ensembles of multiple
125 driver datasets (e.g., weather forecasts; Mercado-Bettín et al., 2021) and parameter sets (e.g.

126 Thomas et al., 2020) to partition and quantify uncertainty (Clayer et al., 2023; Thomas et al.,
127 2020), rather than using multiple models to generate more skillful operational forecasts.

128 Here, we developed a near-term forecasting system that integrates an MME of lake process
129 models, baseline empirical models, and data assimilation algorithms in an automated
130 forecasting approach. We used this MME to produce weekly, 1-14 day-ahead forecasts of water
131 temperature profiles for two years in a small, temperate, drinking water reservoir. We aimed to
132 understand how MME approaches may improve near-term forecast performance and how
133 forecast performance varies over different spatial scales and forecast horizons. We used the
134 MME forecasts to answer the research questions: 1) How does the forecast performance of the
135 process model MME compare to the individual process models?, 2) How does the addition of
136 the baseline models into the MME affect forecast performance?, and 3) How does the forecast
137 performance of the individual models and MMEs vary across horizons and depths? Our goal
138 was to determine if MMEs can improve freshwater water quality forecasting to guide the
139 development of operational forecasting workflows.

140 **2 Methods**

141 2.1 Overview of forecasting system

142 Here, we summarise the automated MME forecasting framework (Figure 1) that leverages the
143 state-of-the-art FLARE (Forecasting Lake And Reservoir Ecosystems) water forecasting system
144 (Thomas et al., 2020). FLARE uses *in situ* water temperature sensor data, which are wirelessly
145 transmitted directly from the waterbody to the cloud, in a data assimilation algorithm to update
146 model initial conditions and to calibrate model parameters (Figure 1; Daneshmand et al., 2021).
147 FLARE's ensemble-based forecasting algorithm generates forecasts using process
148 hydrodynamic models that quantify the uncertainty from driver data (weather forecasts), initial
149 conditions, model process, and model parameters and then samples from these sources of
150 uncertainty to generate probability distributions for water temperature at multiple lake or
151 reservoir depths (see Thomas et al., 2020).

152 Instead of using a single process model, as has been done in previous implementations of
153 FLARE (Carey, Woelmer, et al., 2022; Thomas et al., 2020, 2023), we used three different
154 process models, implemented via integration with *LakeEnsemblR* R software (LER; Moore et
155 al., 2021), to answer question 1. These process models were run inside the FLARE framework

156 to generate a multi-model ensemble (MME) from the output (Figure 1), hereafter referred to as
157 the process model MME forecast (PM MME hereafter). To answer questions 2 and 3, two
158 baseline models were also included to produce the full MME forecast (full MME hereafter),
159 which consisted of five individual models (n=3 process models and n=2 baseline models).
160 Finally, these forecasts are evaluated using the in-situ water temperature observations (Figure
161 1) via a suite of metrics, described below.

162 2.2 Site description and data collection

163 We generated water temperature forecasts for Falling Creek Reservoir (FCR), a eutrophic
164 reservoir located in Vinton, Virginia, USA (37.30°N, 79.84°W). FCR is managed by the Western
165 Virginia Water Authority as a drinking water source. The reservoir has a mean depth of 4 m and
166 a maximum depth of 9.3 m, with a surface area of 0.12 km² (Carey, Lewis, et al., 2022). A
167 dimictic system, FCR generally stratifies from May to October and has intermittent ice-cover
168 from December to March (Carey & Breef-Pilz, 2023). The reservoir has one primary inflow and
169 water level is maintained to be generally constant over time.

170 FCR is monitored by a series of high-frequency sensors deployed at fixed depths in the water
171 column at its deepest site near the dam. Water temperature data were collected using T-Node
172 FR thermistors (NexSens, Fairborn, OH, USA) from March 2019 to March 2023 (Carey et al.,
173 2023; Olsson et al., 2023a), with minor data gaps due to sensor maintenance (see metadata in
174 Carey et al., 2023), across ten depths in the water column (0.0, 1.0, 2.0, 3.0, 4.0, 5.0, 6.0, 7.0,
175 8.0, 9.0 m). Additional temperature data were collected at 1.6 m with a YSI EXO2 sonde (Xylem
176 Inc., Yellow Springs, OH, USA), and at 5.0 and 9.0 m using RDO PRO-X Dissolved Oxygen
177 Sensors (In-Situ Inc., Fort Collins, CO, USA). All measurements were collected at a 10-minute
178 frequency and averaged to an hourly timestep. Observations were then binned into 0.25 m
179 intervals, so that they could be matched with the process model output. When multiple
180 measurements were collected at the same depths, a mean value was calculated. These data
181 were used in FLARE data assimilation and process model parameter tuning, as well as inputs to
182 the two baseline models (see section 2.3), and in forecast evaluation (Figure 1, section 2.4).

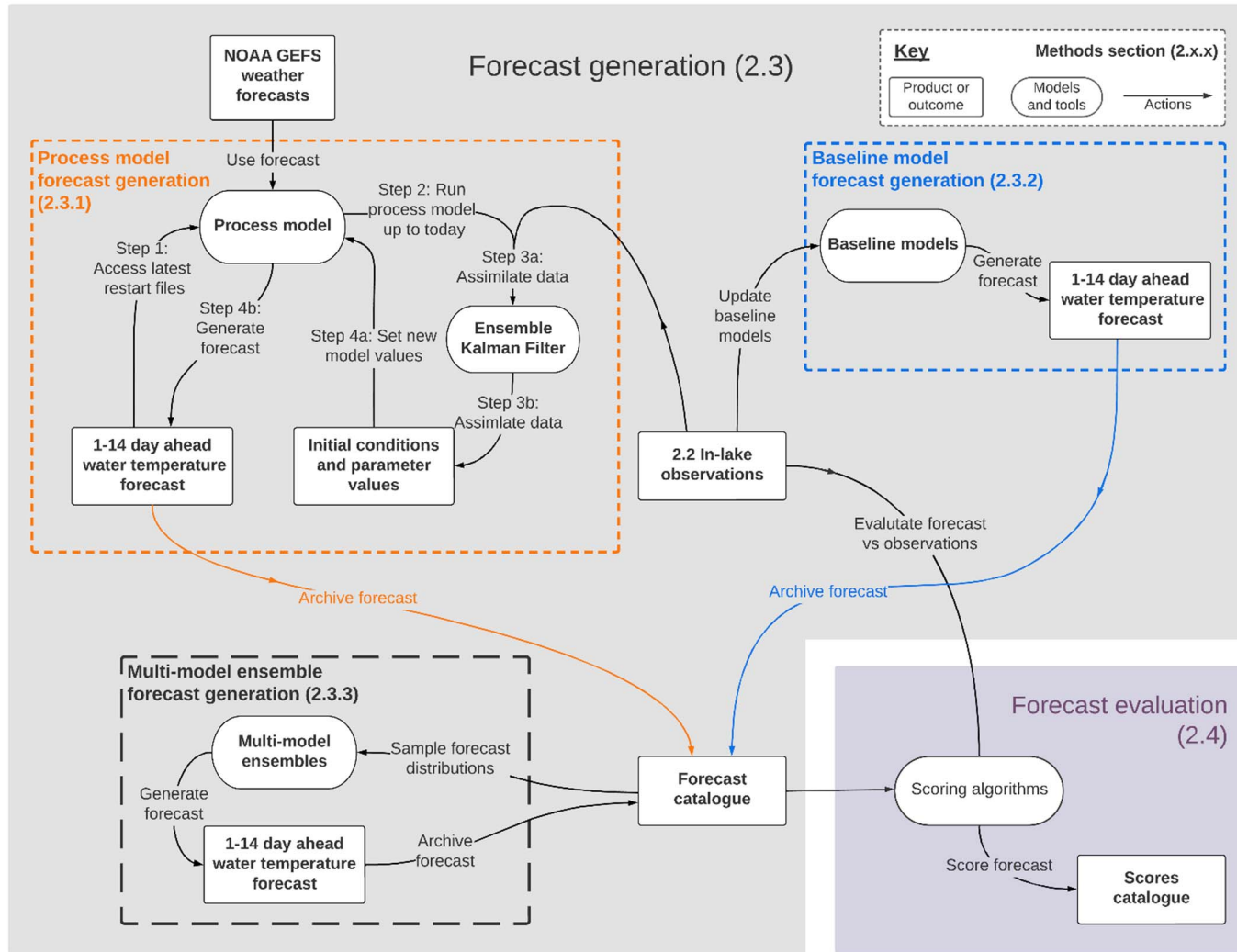


Figure 1. Multi-model ensemble and individual forecast generation (grey shading) and forecast evaluation workflow (purple shading), with each corresponding text section number in parentheses (e.g., 2.3). Boxes represent tools, objects, and/or products and lines represent actions. The parallel workflows of individual model forecast generation are shown in the orange (process models) and blue (baseline models) boxes. Within the process model forecast workflow, the steps correspond to the text in section 2.3.1. Each individual model forecast is archived into the *Forecast Catalogue* from which the distributions are sampled and combined in the multi-model ensemble (black dashed box). The multi-model ensemble forecasts are also archived in the *Forecast Catalogue*. From this catalogue, forecasts are evaluated against in-lake observations via several scoring algorithms to generate a *Scores Catalogue*, which is subsequently analysed (section 218.2.4).

183

184

219 Dates of the mixed and stratified periods were calculated based on the density difference
220 between 1 m from surface (1 m) and ~1 m above the bottom (8 m) of the lake, with a minimum
221 density difference of 0.1 kg m⁻² indicating that the lake was stratified (Wilson et al., 2020). The
222 stratified period was defined as the summer period when continuous stratified conditions
223 occurred and the mixed period as any time outside of this. In addition, the observed thermocline
224 depth was estimated using the *LakeAnalyzer* R package (Read et al., 2011).

225 2.3 Forecast generation

226 2.3.1 Process model forecasts

227 In this application, FLARE generated forecasts for each of the three process models every
228 seven days for 1 to 14 day-ahead horizons over 2 years (March 2021 - March 2023), resulting in
229 a total of n=104 forecasts per model. For each process model, the weekly forecasts were
230 generated using the following steps (Figure 1): Step 1) access the individual FLARE forecasts
231 (Figure 1, step 1) for 1-week ago in a prior FLARE run (or, in the case of the first forecast,
232 following a spin-up described below); Step 2) use this prediction to initialise each process model
233 FLARE run that starts 1-week ago and runs to current day (Figure 1, step 2); Step 3) use a data
234 assimilation algorithm (the ensemble Kalman filter; Evensen, 2003) to assimilate new
235 observations collected over the past week (Figure 1, step 3) to update that model's states and
236 parameters (Figure 1, step 3); and Step 4) use the updated states and parameters as initial
237 conditions for a 1- to 14-day ahead forecast that starts today (Figure 1, step 4). Each forecast
238 included 256 simulations (ensemble members) that quantified the uncertainty from driver data
239 (weather forecasts), initial conditions, model process, and model parameters. Additional
240 information about FLARE configuration can be found in Thomas et al., (2020) and Thomas et al.
241 (2023).

242 Within the FLARE framework, three process models were implemented using the
243 *LakeEnsembIR* R package (LER; Moore et al., 2021), and underwent data assimilation within
244 FLARE as described above. This R package facilitates the running of up to five one-dimensional
245 hydrodynamic lake models simultaneously using the same driving data and configuration files
246 (see Moore et al. 2021). The three process models we included in the PM MME were the
247 General Lake Model (GLM; Hipsey et al., 2019), General Ocean Turbulence Model (GOTM;
248 Umlauf et al., 2005), and Simstrat (Goudsmit et al., 2002), hereafter referred to as PM1, PM2,
249 and PM3, respectively. The other two process models implemented in LER (FLake, MyLake)

250 were not included because our aim was to apply data assimilation and iteratively forecast full
251 water column temperature profiles. Specifically, FLake simulates lake systems using a two-layer
252 representation (Mironov, 2021) that does not simulate a full profile, and MyLake is not able to
253 “restart” daily (Saloranta & Andersen, 2007), as needed for iterative forecasting with data
254 assimilation.

255 All three process models require forecasted meteorological driving data to produce water
256 temperature forecasts. To make near-term predictions of water temperature, we used weather
257 forecasts for FCR from the National Oceanic and Atmospheric Administration's (NOAA's) Global
258 Ensemble Forecast System (GEFS; Hamill et al., 2022). The NOAA GEFS weather forecast
259 consists of a set of 31 simulations and a forecast horizon of 1 to 16 days-ahead, which we used
260 to produce 1-14 day-ahead water temperature forecasts from the midnight UTC data product.

261 We followed the standardised FLARE configuration for forecasting (Thomas et al., 2023). All
262 process models were run at an hourly time step with the midnight output as the daily forecast. A
263 spin-up of all models was run from 1 October 2020 to 1 March 2021, the date of the first
264 forecast. During this spin-up, each model's parameters were individually tuned by the ensemble
265 Kalman filter within FLARE (see Supplementary Information, Table S1, Figure S1). Each model
266 used default parameters to initialise the forecast run and two sensitive parameters were tuned in
267 the data assimilation process of FLARE (See Supplementary Information, Table S1, Figure S1).
268 The sensitive parameters selected, based on initial investigation and configuration in other
269 lakes, were the sediment temperature and incoming shortwave radiation scaling factor for GLM,
270 and the wind scaling and incoming shortwave radiation factors for Simstrat and GOTM (see
271 Supplementary Information).

272 2.3.2 Baseline models

273 Two simple, empirical baseline models were also used to generate forecasts (Figure 1). The
274 persistence model uses the last observation for each specific depth as a prediction of future
275 conditions and the climatology model uses a long-term day-of-year mean as the daily forecast
276 (Hyndman & Athanasopoulos, 2021; Jolliffe & Stephenson, 2012); both are described in detail
277 below.

278 2.3.2.1 Persistence model

279 A persistence model assumes that, on average, the forecasted state (in this case, water
280 temperature) on average does not change over the forecast horizon, with uncertainty driven by
281 a random walk process (Hyndman & Athanasopoulos, 2021):

$$282 \quad y_{T+1} = y_T + e_{T+1} \text{ (Eqn. 1)}$$

283 where y_T is today's observation or forecast, e_{T+1} is random noise, and y_{T+1} is the next day's
284 forecast. The uncertainty (e_{T+1}) in the persistence model forecasts were generated using a
285 bootstrapping method, as a normal distribution could not be assumed. The bootstrap method
286 calculates the distribution of residuals from the fit and samples from that distribution for a value
287 of e_{T+1} . We used bootstrapping to generate a set of $n=256$ ensemble members to match the
288 number of simulations as the process models. The persistence model forecasts were generated
289 using the *RW* (random walk) function in the *fable* R package (version 0.3.2; O'Hara-Wild et al.,
290 2022).

291 2.3.2.2 Climatology model

292 A climatology model, also based on historic observations, was used to generate a forecast,
293 assuming forecasted mean conditions are equal to the historic day-of-year mean. We used two
294 years of observations (March 2019 - March 2021) from FCR to calculate a day-of-year mean
295 water temperatures at each depth. We chose this period because the thermistor sensors were
296 deployed in summer 2018 and we wanted to ensure that each day-of-year mean water
297 temperature was derived from the same number of historical observations. To obtain uncertainty
298 around these climatology forecasts, we fitted a linear model between the two years of
299 observations and calculated the standard deviation of the residuals, at each depth
300 independently. We generated the probabilistic climatology forecasts by sampling from a normal
301 distribution with the obtained mean and standard deviation, generating $n=256$ ensemble
302 members.

303 2.3.3 Multi-model ensembles (MMEs)

304 As described above, we generated two MMEs: the PM MME (containing PM1, PM2, PM3; $n = 3$
305 models total) and the full MME that also included the two baseline models (persistence,
306 climatology; $n = 5$ models total). To create the full MME forecasts, the $n=256$ ensemble

307 members from each of the three individual process models and two baseline models were
308 combined into a new MME (Figure 1). As the number of simulations generated from forecast
309 can affect forecast skill (Machete & Smith, 2016), we sampled from the pool of individual model
310 simulations to generate MMEs with $n=256$ ensemble members, with each model equally
311 represented. The number of simulations from each individual model in the MME forecasts is
312 given as $256/n$, where n is the number of models in the MME. For example, in the full MME
313 there were 5 models represented in the forecast, giving 51 simulations ($256/5$) from each
314 individual model.

315 2.4 Forecast evaluation

316 Forecasts from both the individual models and MMEs were evaluated using four evaluation
317 metrics calculated on each forecast-observation pair. We used multiple evaluation metrics
318 because each metric provides complementary information about the performance of the
319 forecast. First, we calculated the mean bias (difference in mean forecasted water temperature
320 and observed water temperature). Forecasts with lower bias indicate increased forecast
321 accuracy. Second, we calculated the standard deviation (SD) of the forecasts to understand
322 uncertainty in the forecasts. We expect uncertainty to increase across the forecast horizon as
323 confidence in future conditions decreases. We also expect to see larger SD in the MME
324 forecasts than individual model forecasts as they reflect a greater diversity of predictions. Both
325 metrics are useful for determining how the forecast accuracy (bias) and precision (using SD as
326 a metric of uncertainty) vary independently and are commonly calculated metrics for forecast
327 performance (Jolliffe & Stephenson, 2012).

328 Third, we evaluated the models using the ignorance score (IGN), which uses both the accuracy
329 and the precision of the forecasts in its evaluation, and describes the probability placed by the
330 forecast on the observed outcome (Smith et al., 2015). IGN was calculated using the
331 *scoringRules* R package (Jordan et al., 2019), in which larger values represent a lower
332 probability placed on the observed outcome and lower forecast performance. IGN, originally
333 proposed by Good (1952), is defined as:

$$334 \quad \text{IGN}(p(x), X) = -\log_2(p(X)) \text{ (Eqn. 2)}$$

335 where $p(x)$ is the density assigned to the outcome X .

336 IGN penalises forecasts that place very low probabilities on the observed outcome and gives an
337 infinitely large score if a forecast places zero probability on an outcome that is ultimately
338 observed (Smith et al., 2015). We selected the IGN score as a focal evaluation metric because
339 differences in scores between models represent the additional probability placed on the
340 observed outcome in the more skillful forecast (Smith et al., 2015). The difference in IGN scores
341 between two models can be used as the exponent of base two to calculate the probability
342 difference between the models (Smith et al., 2015). For example, an IGN score difference of 0.5
343 units between two models corresponds to the better model placing $2^{0.5}$, or 1.41 times more
344 probability, on the more skillful forecast. Thus, in this example, there is a confidence gain of
345 41% in the better model compared to the other model (Smith et al., 2015).

346 Finally, we calculated shadowing time, which quantifies the time that the forecast is able to
347 “shadow” the observations, given an estimate of observational uncertainty (Gilmour & Smith,
348 1997; Smith et al., 2010). The shadowing time is the maximum number of consecutive days,
349 starting from forecast initiation, that at least one simulation (ensemble member) tracks the mean
350 observation, within a specified observation uncertainty. Here, we define a simulation as
351 shadowing when it falls within the 95% confidence interval of each observation (assuming a
352 normal distribution centred on the observation). Observational uncertainty (standard deviation)
353 was estimated at 0.2°C, based on an analysis of the variation in observations within each day
354 and depth (see Supplementary Information, Figure S2). Shadowing time is a useful metric to
355 determine how well the forecast models can replicate the dynamics of a system, rather than the
356 statistics of the forecast (Gilmour & Smith, 1997; Smith et al., 2010).

357 2.5 Analyses

358 First, to address question 1, we compared the evaluation metrics among the individual process
359 model forecasts and the PM MME forecast. Second, to address question 2, we compared the
360 full MME with the PM MME, and the performance of the five individual process models and
361 baseline models. To understand how and why the MME forecasts might be able to outperform
362 individual models, we also calculated the Pearson correlation coefficient (r) on forecast bias.
363 Third, to address question 3, we compared the forecast metrics at different depths and forecast
364 horizons. We also determined each model’s rank (out of the 7 forecasts from the 5 individual
365 and 2 MMEs) for each individual forecast-observation pair across depth and horizon using the

366 IGN score. All analyses were conducted using R statistical software (v.4.2.1; R Core Team,
367 2021).

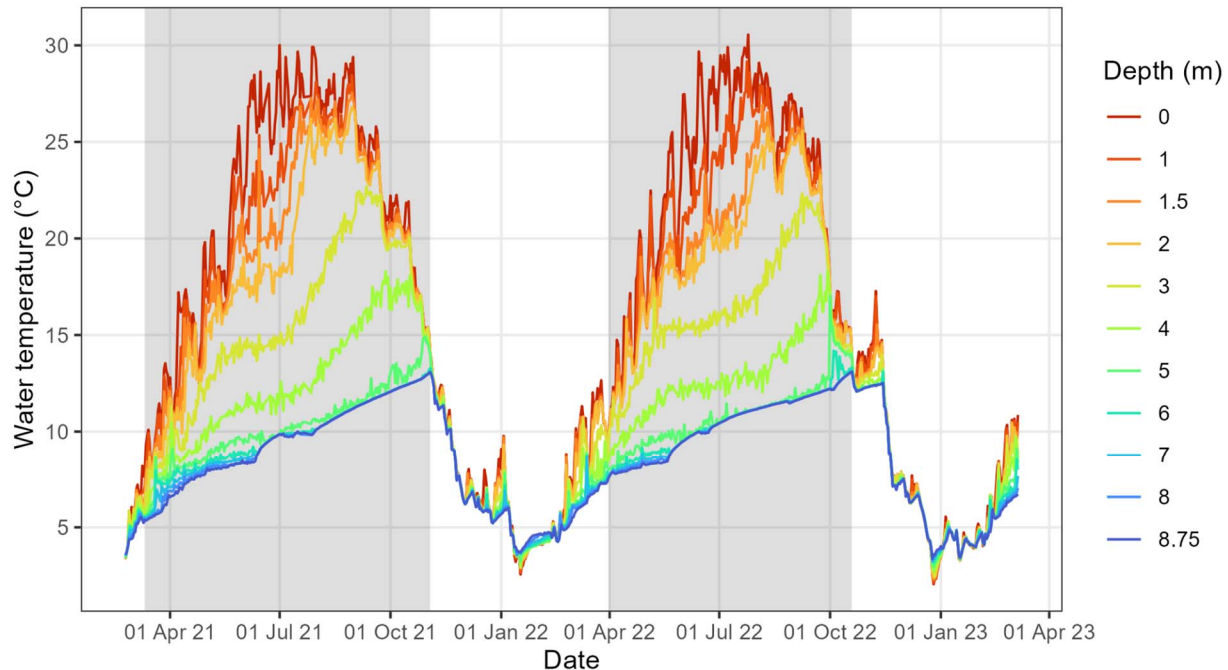
368 2.6 Archiving

369 All data and code are archived and available in the Zenodo repositories (Olsson et al., 2023a,
370 2023b) or the Environmental Data Initiative repositories (Carey et al., 2023; Carey & Breef-Pilz,
371 2023). Instructions on reproducing the individual model forecasts as well as the multi-model
372 ensemble are available in (Olsson et al., 2023b). In addition, the forecasts and scores can be
373 accessed here to enable the manuscript figures to be reproduced (Olsson et al., 2023a).

374 **3 Results**

375 3.1 Observed and forecasted temperature dynamics at FCR

376 FCR exhibited typical seasonal dynamics during the two-year forecasting period. Continuous
377 summer thermal stratification lasted from 11 March - 3 November 2021 and 31 March - 19
378 October 2022. Outside of these periods, there were transient periods of mixing and stratification
379 during spring and autumn (Figure 2). Ice cover was observed intermittently during the periods of
380 11 January - 8 February 2022 and 23 December 2022 - 6 February 2023. As ice cover was
381 short and intermittent, we hereafter refer to the period outside of the summer stratified period as
382 'mixed,' despite brief periods with inverse thermal profiles (Figure 2). Mean thermocline depth
383 during the summer stratified period was 2.7 m in 2022 and 3.1 m in 2023.

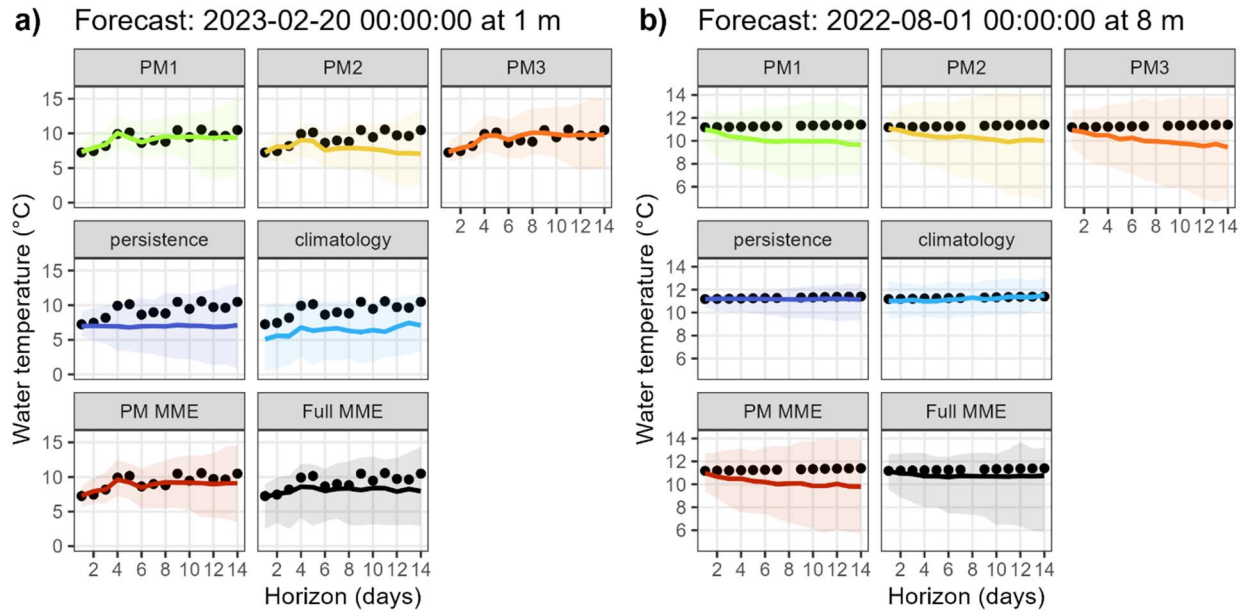


384
 385 Figure 2. Observed high-frequency water temperatures across eleven depths at Falling Creek
 386 Reservoir from March 2021 to March 2023. The grey shaded areas show the periods of
 387 continuous summer stratification and white shaded areas show the mixed periods.

388 Our workflow (Figure 1) was able to successfully produce weekly 1-14 day-ahead forecasts for
 389 the two-year forecasting period for all five individual models and the two MMEs (Figure S3). In
 390 general, mean forecast performance was highest at the beginning of the forecast horizon and
 391 decreased further into the 14-day-horizon (Figure S3). Across all depths and horizons, the IGN
 392 score of the individual models (other than climatology) increased by 80-170% from 1 to 14 days-
 393 ahead, representing lower performance. Forecast uncertainty also increased across the 14-day
 394 horizon for all models except for climatology (by >100%).

395 Two examples highlight how the forecasts generated by the individual models exhibited
 396 differences in how well they reproduced observations across depths and times (Figure 3). First,
 397 forecasts generated during the mixed period at 1 m depth (20 February 2023) show that PM1
 398 and PM3 forecasts closely followed observations throughout the 1 to 14-day ahead horizon, with
 399 PM2 diverging from observations after the 8th day of the forecast horizon. In contrast, the
 400 climatology and persistence baseline models consistently underestimated water temperature. In
 401 a second period with stratified water temperatures (1 August 2022), forecasts generated at 8 m
 402 depth show that PM3, and to a lesser extent PM1 and PM2, underestimated the water
 403 temperature. The two baseline models were most skillful for this particular forecast.

404 The variable performances of the individual models are reflected in the performance of the two
 405 MME forecasts (Figure 3). For example, in the first example forecasts for 20 February 2023 at 1
 406 m depth, the PM MME performed better than the full MME because of the superior performance
 407 of the process models than the baseline models. Likewise, in the second example forecasts for
 408 1 August 2022 at 8 m, the full MME performed better than the PM MME because of the strength
 409 of the baseline models.



410
 411 Figure 3. Two example water temperature forecasts from the five individual models and the two
 412 multi-model ensembles: one generated on 20 February 2023 at 1 m depth (mixed period; left
 413 panels) and one generated on 1 August 2022 at 8 m depth (stratified period; right panels). The
 414 top row shows the individual forecasts from the three process models (PMs), the middle row
 415 shows the individual forecasts from the two baseline models, and the bottom row shows the
 416 multi-model ensembles (PM and full MMEs). Shaded areas show the 95% confidence interval
 417 around the median forecast (line) and the filled points are the observed water temperatures. The
 418 colours for the different forecasts are consistent throughout.

419 3.2 Question 1: How does the performance of the process model MME compare to the
 420 individual process models?

421 Overall, the PM MME exhibited a higher aggregated performance, as determined by the lowest
 422 absolute bias and ignorance score, than the individual PMs (Table 1; Figure 4). When
 423 aggregated across all forecast dates, horizons, and depths, the bias of the PM MME was similar
 424 to PM1, highlighting how the addition of the other two PMs with slightly higher absolute bias did
 425 not increase bias in the MME (Table 1). The bias increased over the 1-14 day forecast horizon
 426 for all PMs and the PM MME, with bias increasing less for the PM MME and PM1 (Figure 4a). In

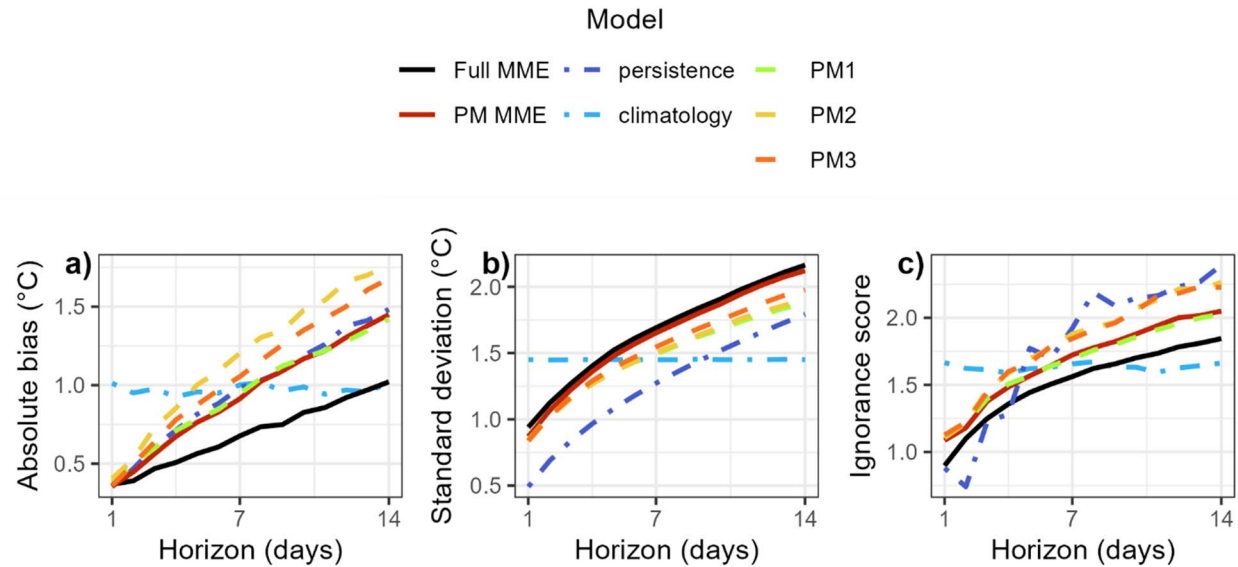
427 contrast to bias, the PM MME had a larger mean forecast uncertainty (SD) than any of the
 428 individual models, especially at longer horizons (Figure 4b). SD increased over the forecast
 429 horizon at a faster rate for the PM MME than any individual PM (Figure 4b). At 1 day-ahead, the
 430 SD was similar for all PM forecasts (1.1°C), but by 14 days-ahead, the PM MME had 0.2°C
 431 higher SD than the best individual PM forecast (Fig. 4b).

432 Table 1. The mean ignorance score (IGN), absolute bias, standard deviation (SD), and
 433 shadowing time aggregated for all forecasts across all depths, times, and horizons for each
 434 forecast model, individual and multi-model ensemble (MME) across the two-year forecasting
 435 period. Models are sorted by most to least skillful, based on IGN, with the “best” forecast based
 436 on each metric in **bold**.

Forecast model	IGN	Absolute Bias (°C)	SD (°C)	Shadowing time (days)
Full MME	1.52	0.69	1.66	7.3
Climatology	1.63	0.98	1.45	3.2
PM1	1.67	0.95	1.47	4.5
Process model MME	1.68	0.94	1.62	4.2
PM2	1.80	1.16	1.49	3.7
PM3	1.81	1.09	1.53	4.0
Persistence	1.89	0.98	1.26	7.9

437 When using the IGN metric to evaluate performance, which combines accuracy and precision,
 438 the PM MME performance was similar but slightly lower than the performance of PM1 (Table 1).
 439 This result highlights the penalty given by the IGN score to the higher standard deviation in the
 440 PM MME. The best performing PM only placed 9% more probability on the observed outcome
 441 than the worst PM forecast on average, and 1% more probability than the PM MME (Equation
 442 2). IGN increased over the forecast horizon at a similar rate for both the PM MME and most
 443 skillful individual forecast (PM1, Figure 4). At 14 days-ahead, the PM MME placed 13% more
 444 probability in the observed outcome and PM1 16% more probability than the two other individual
 445 forecast models. This change in probability demonstrates that the MME is not penalised strongly
 446 for including the “worse” models overall (Figure 4).

447 Using the shadowing time metric, the PM MME did not show increased ability to replicate
 448 observed water temperature dynamics relative to the individual models. The mean shadowing
 449 time for the PM MME (4.2 days) was slightly shorter than the best PM (4.5 days; Table 1).
 450 Shadowing time for the other PMs (PM2 and PM3) were shorter than the PM MME but all were
 451 between 3.7 and 4.5 days, less than half of the total forecast horizon.



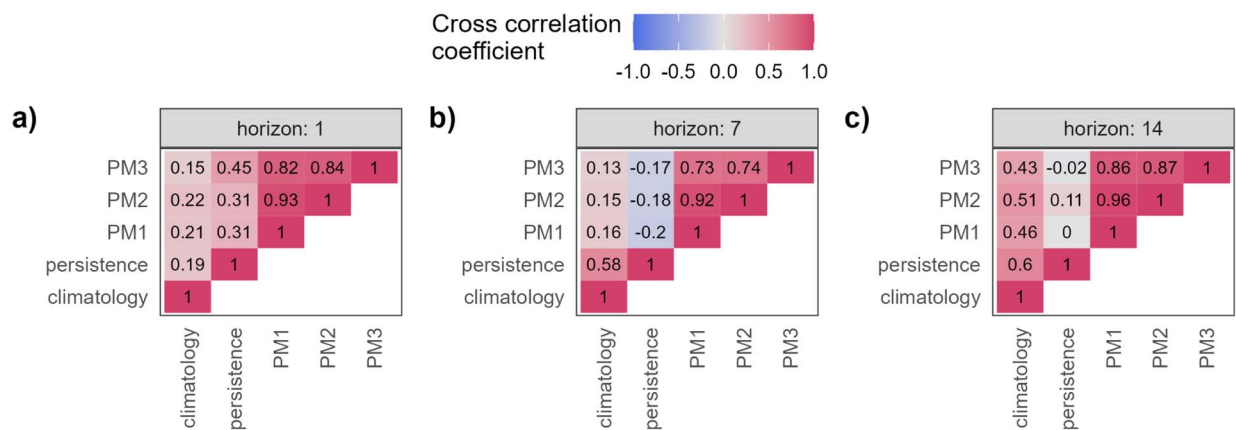
452
 453 Figure 4. a) Mean absolute bias, b) standard deviation, and c) ignorance score across the 14-
 454 day forecast horizon for the three individual process models (PM), two baseline models
 455 (climatology and persistence), and the process model multi-model ensemble (PM MME) and full
 456 multi model ensemble (full MME).

457 3.3 Question 2: How does the addition of the baseline models into the full MEE affect
 458 forecast performance?

459 Altogether, the full MME had the lowest IGN, lowest bias, and highest standard deviation of any
 460 individual model or MME (Table 1). Aggregated across all depths, times of year, and horizons,
 461 the inclusion of the two baseline models into the full MME decreased bias by 26% but only
 462 increased the standard deviation by 2% (Table 1), relative to the PM MME. This large reduction
 463 in bias led to a lower IGN for the full MME (vs. the PM MME) despite the slight increase in
 464 uncertainty. Using the difference in the IGN metric, the full MME placed 12% more probability on
 465 the observed outcome than the PM MME. Overall, the improvement in performance of the full
 466 MME relative to the PM MME increased throughout the forecast horizon (Figure 4a), a 6%
 467 improvement at 2 days-ahead compared to 15% at 14 days-ahead.

468 The shadowing time of the full MME (7.3 days) was longer than the PM MME (4.2 days; Table
 469 1). This improvement in shadowing time was due to the inclusion of the persistence model in the
 470 full MME. The persistence model had the longest shadowing time of any individual model or
 471 MME (7.9 days).

472 The individual PM forecasts exhibited high covariance with other PM forecasts and low
 473 covariance with the baseline model forecasts (Figure 5). At 1 m, the PM models exhibited strong
 474 positive correlations at 1, 7, and 14 day-ahead horizons ($r = 0.73$ to 0.96), with PM1 and PM2
 475 being most correlated at these three horizons. In contrast to the individual PM models, the
 476 individual baseline models generally showed low covariance between each other and with the
 477 PM models (Figure 5). A few exceptions to this pattern were at 1 day-ahead, when the
 478 persistence model showed a moderate correlation with PM3 ($r = 0.45$) at 1 m. Similarly, at 7 and
 479 14 days-ahead, the persistence and climatology showed a positive correlation ($r = 0.58$ and $r =$
 480 0.60 , respectively), and at 14 days-ahead the climatology model was positively correlated with
 481 all other models. The correlations among the PMs were always higher than any correlation
 482 involving a baseline model (Figure 5).



483 Figure 5. Correlation (Pearson r) of bias among individual model forecasts. The correlation
 484 coefficient between models was calculated for the mean forecast bias (mean - observations) at
 485 1, 7, and 14 day-ahead horizons for 1 m. Red indicates a strong positive correlation and blue
 486 indicates a strong negative correlation.
 487

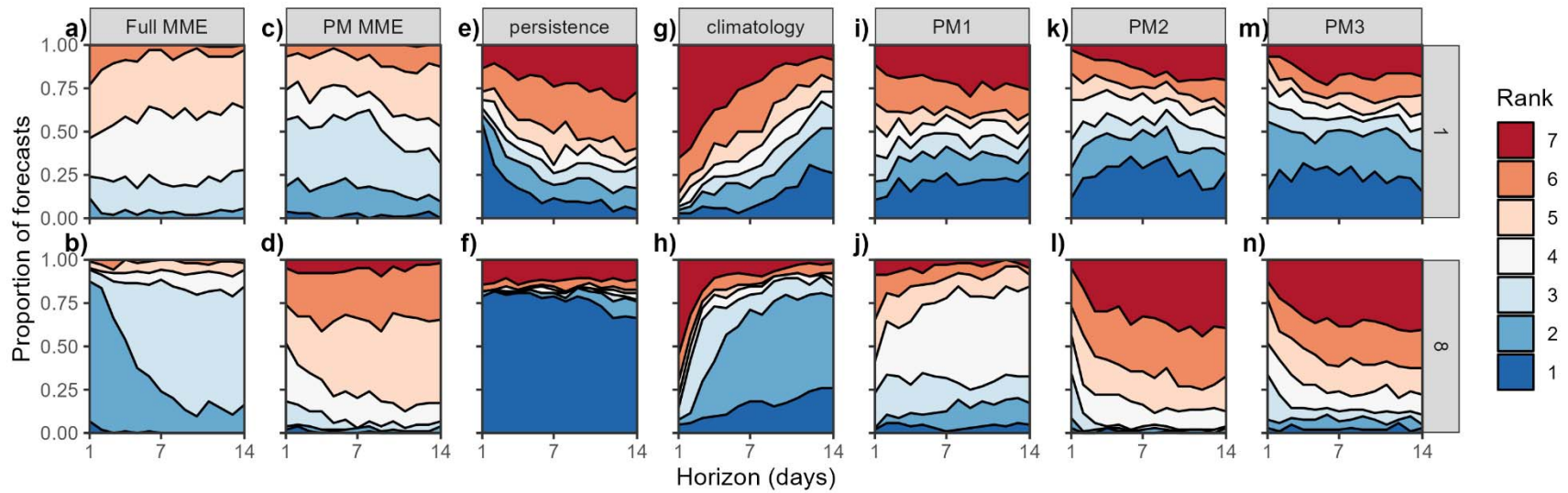
488 3.4 Question 3: How does the forecast performance of the individual models and MMEs vary
 489 across horizons and depths?

490 The ranking of models demonstrates the hedging that occurs when using MMEs to forecast at
 491 different depths and horizons. The individual model forecasts were more likely to be ranked the
 492 'worst' of the seven forecasts (Figure 6, Figure S4) than the two MME forecasts. Out of all
 493 $n=104$ forecasts generated, the full MME had $<1\%$ of rank 7 (worst) forecasts across 1 and 8 m
 494 ($n=1$ forecast) and 10% of rank 1 (best) forecasts ($n=11$). At 1 m, the full MME was most often
 495 ranked in the middle (65-95% of forecasts ranked 3-5, respectively; Figure 6a). At 8 m, the full
 496 MME was more often ranked the second-best forecast, especially at shorter horizons (Figure

497 6b), with more than 50% of forecasts at ranks 1 or 2 up to 4 days-ahead. Despite the decrease
498 in high-ranking forecasts (ranks 1-2) at longer horizons, there was no appreciable increase in
499 the proportion of worst-ranking forecasts (ranks 6-7), remaining between 2-6% of forecasts at
500 most horizons.

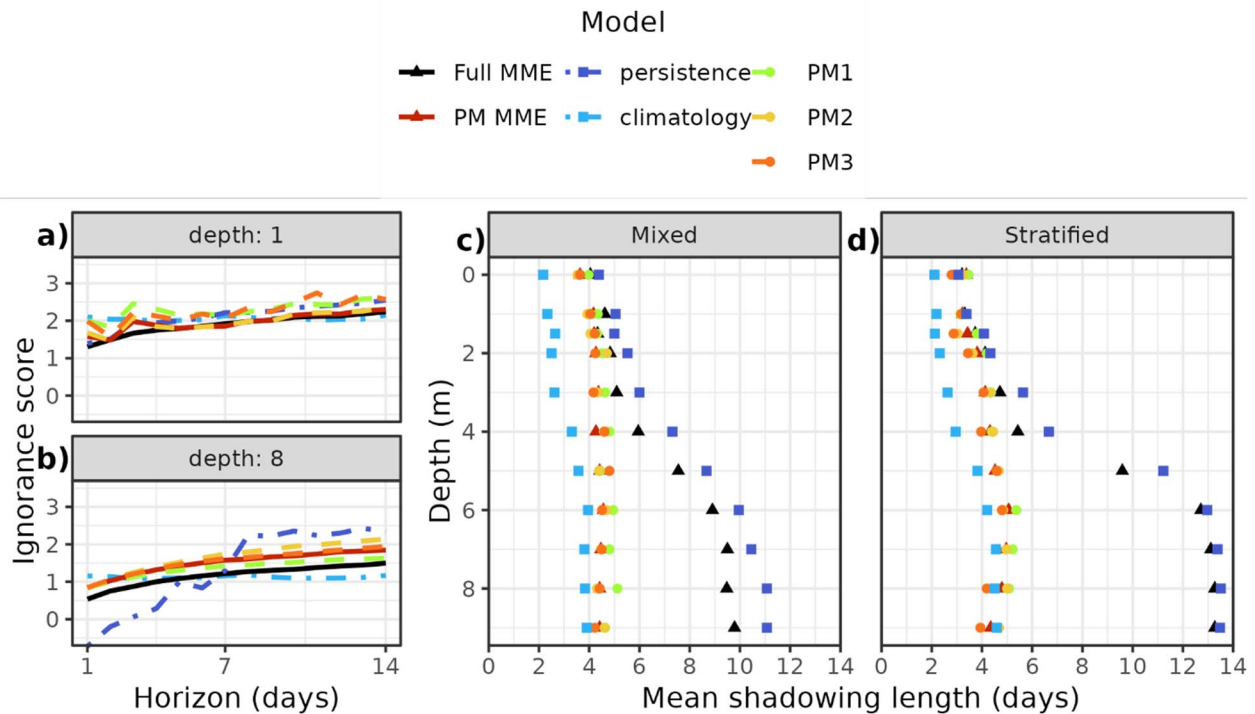
501 The individual PM forecasts were dominated by rankings of either the best (1) or worst (7)
502 performance, whereas the PM MME had fewer of these extreme ranks. At 1 m, the individual
503 PM models had almost equal proportions of rank 1 and rank 7 forecasts across the full horizon
504 (Figure 6i,k,m), with over 40% of forecasts ranked at one of these extremes, compared to only
505 2% of the PM MME forecasts exhibiting one of these extreme ranks. At 8 m, the individual PM
506 models were more often at an intermediate rank than at 1 m (Figure 6j,l,n), although PM2 and
507 PM3 had more than 40% of the worst forecast, whereas PM1 had up to 56% of forecasts with
508 an intermediate rank and fewer very poor forecasts (rank=7).

509 The ranks of the baseline models varied substantially at different depths and horizons. At 1 m,
510 the persistence model had more than 50% of forecasts in rank 1 for 1 day-ahead forecasts,
511 which declined steeply to only 10% at horizons >5 days-ahead (Figure 6e). Concurrently, the
512 proportion of forecasts for which persistence was the worst forecast also increased across the
513 forecast horizon, with more than 50% of the forecasts having persistence at ranks 6 or 7
514 forecast at 13-14 days ahead (Figure 6e). At 8 m, the persistence forecasts dominated the best
515 performing rank across the whole horizon (Figure 6f), only decreasing marginally from around
516 80% to 65% of total forecasts by 14 days-ahead (Figure S4). The climatology model
517 demonstrated strengths at longer horizons at both 1 and 8 m. The proportion of climatology
518 forecasts at 1 m with a rank 1 increased across the forecast horizon, from <5% at 1 day-ahead
519 to 26% of forecasts at 14 days-ahead (Figure 6g). However, climatology was frequently the
520 least skillful forecast at 1 m, especially at 1 day-ahead (Figure S4; 65% of forecasts). At
521 horizons between 3 and 10 days-ahead, 40% of the climatology forecasts were either the first or
522 second ranked forecast, which increased to 80% at horizons >10 days-ahead.



523
 524 Figure 6. Proportion of total forecasts ($n = 104$) with each rank, from 1 (best) to 7 (worst), out of the five individual models and two
 525 multi-model ensembles (process model (PM) and full MMEs). Ranks were calculated for each individual forecast ($n = 104$) and each
 526 horizon (1 to 14 day-ahead) based on the ignorance forecast metric at 1 m (top row) and 8 m (bottom row) depths.

527 Inspection of the disaggregated forecast scores further demonstrates that there was no one
 528 consistently best-performing model or MME at all horizons and all depths, as determined by IGN
 529 scores and shadowing times (Figure 7a,b). At 1 m, the two MME forecasts had the highest skill
 530 across the total horizon (Table S2), although they were outperformed at certain horizons by the
 531 individual PM2 model and, beyond 10 days-ahead, climatology (Figure 7a). Conversely, at 8 m,
 532 the persistence model had the best performance for 2 days-ahead, the full MME exhibited the
 533 best performance 1 and 3-5 days-ahead, and then the climatology model had the highest skill
 534 up to 14 days-ahead (Figure 7b).



535 Figure 7. Disaggregated forecast performance (ignorance score) at 1 (a) and 8 m (b) for each
 536 and mean shadowing time at each observed depth in the water column in the mixed (c) and
 537 stratified periods (d) for the three individual process models (PM), two baseline models
 538 (climatology and persistence), and the process model (PM) MME and full MME.
 539

540 As with the aggregated shadowing times, including the baseline models in the full MME
 541 extended the shadowing time compared to the PM MME at almost all depths during both the
 542 stratified and mixed periods (Figure 7c, d). The persistence model had the longest shadowing
 543 time across all forecasts (mean = 7.9 days, Table 1), which was consistent across depths,
 544 except for forecasts at the surface (0 m) during the stratified period (Figure 7d). The persistence
 545 model showed significantly better shadowing ability than the other individual model forecasts,
 546 especially at depths deeper than 4 m, which corresponded to depths below the thermocline,

547 calculated at a depth of 2.7-3.1 m during the forecast period. For example, at 5 m, the
548 shadowing time of the persistence forecast during the stratified period was 2.5 times longer than
549 the next best individual model (PM1). The shadowing time of the PM MME did not improve on
550 the best individual model (PM1), although all PM showed low shadowing ability (<6 days at all
551 depths) relative to the persistence and full MME. At 8 m, both the persistence model and the full
552 MME were able to almost shadow the full horizon (Figure 7d; mean shadowing times = 13.5 and
553 13.2 days, respectively).

554 **4 Discussion**

555 Reservoir water temperature forecasts generated using a multi-model ensemble (MME)
556 consisting of process and baseline models performed better overall than using individual models
557 or a process model (PM) MME. Our results support previous research that shows that MME
558 methods often outperform individual models (Atiya, 2020; Johansson et al., 2019; Viboud et al.,
559 2018). For example, in a large diverse forecasting competition of multiple finance and
560 demography variables, 70% of the most accurate forecasts were MMEs (Atiya, 2020). Our
561 results showed that no individual model performed best at all depths and horizons, as the best
562 models at 1 m (the individual process models) were the worst performers at 8 m. In contrast to
563 this finding, the full MME was rarely the worst-performing forecast, highlighting the hedging
564 ability of MMEs to prevent very poor forecast performance (Atiya, 2020). MMEs incorporate the
565 strengths of multiple models given that all models are likely imperfect representations of reality
566 (Atiya, 2020) as well as acknowledging the between-model uncertainty (Humphries et al., 2018).
567 Below, we examine some of the implications for using MME forecasts and highlight ways to
568 further improve MME forecasts for other applications.

569 **4.1 No one individual model is optimal for all forecast horizons or depths**

570 For individual 1-14 day-ahead forecasts at specific horizons and depths, individual models
571 outperformed the MMEs (Figure 7), accounting for >96% of the best forecasts at 1 m and >91%
572 at 8 m (Figure S4). Each model captures slightly different dynamics of the mechanistic
573 processes controlling reservoir water temperature and therefore performed optimally under
574 different conditions (Lapeyrolerie & Boettiger, 2023). This was also observed in a multi-model
575 river forecasting study in which individual models alternately performed best in predicting
576 different stages, phases, or mechanisms of rainfall-runoff (Abrahart & See, 2002) and a penguin

577 population forecasting study in which a range of models differentially captured inter-annual and
578 inter-species variability (Humphries et al., 2018). Altogether, our study contributes to the
579 evidence that combining forecasts from different models provides a more comprehensive and
580 accurate representation of the forecasted system than one model alone.

581 In our analysis, the optimal model varied by depth and horizon, demonstrating the individual
582 strengths of each model. The persistence forecast was significantly better across all horizons at
583 8 m than other models (ranked best in 66 - 82% of all forecasts, Figure 6e), but generally
584 performed poorly at 1 m at horizons beyond 1 to 2 days-ahead (Figure 7). This finding is in
585 agreement with a previous water temperature forecast study at the same reservoir, which found
586 high forecast skill from a persistence model deeper in the lake and higher skill from a PM at the
587 surface (Thomas et al., 2020). Individual PMs have been shown to be successful at forecasting
588 water temperature dynamics at the lake surface at short horizons (Thomas et al., 2020; Wander
589 et al., 2023). As weather forecast skill degrades further into the future, there is a subsequent
590 reduction in water temperature forecasting skill at these shallower depths at longer horizons
591 (Carey, Woelmer, et al., 2022; Thomas et al., 2020). This pattern is likely because
592 meteorological driver data uncertainty has been shown to be the primary source of uncertainty
593 in surface water temperature forecasts, due to the sensitivity of surface water temperatures to
594 atmospheric forcing (Thomas et al., 2020).

595 One promising approach for better utilising the strengths of the individual models is to weight
596 the individual models within the MME based on their historical forecast performance. Weighting
597 the individual models may further increase MME skill (reviewed by Wang et al., 2022), as these
598 methods seek to exploit the inherent benefits of each individual model represented in the MME
599 (Abrahart & See, 2002). MME blending methods that weight accurate models more highly and
600 adjust weights dynamically may leverage the strengths of the models whilst minimising their
601 weaknesses (Chandler, 2013; Spence et al., 2018). For example, Abrahart & See (2002) used a
602 fuzzy logic approach to use the previous forecast performance to weight the models used in the
603 next forecast MME when forecasting river flow. However, selecting the optimal MME blending
604 method was dependent on the dynamics of the flow conditions (Abrahart & See, 2002). Wang et
605 al. (2022) note in their review that simple combination methods, such as the linear pooling with
606 equal weights (as done here) or simple averaging, are some of the most robust approaches for
607 model blending and that improvements from optimised weights can be outweighed by the error
608 added by estimating these parameter values (Dormann et al., 2018). In short, estimating the

609 weighting parameters adds another source of uncertainty to the forecasts whereas simple
610 averaging is robust and easier to implement (Barrow & Kourentzes, 2016). A potential
611 alternative to applying a weighting method would be to identify a suitable pool of models to use
612 in the MME and omit the worst performing ones, thus diminishing the worst predictions within
613 each individual model forecast (Abrahart & See, 2002; Dormann et al., 2018), unless it is very
614 diverse from the other models (Atiya, 2020).

615 4.2 The PM MME did not significantly improve on the best individual process model

616 When aggregating the ignorance score across all forecasts, the PM MME performed slightly
617 worse than the best individual PM model. However, the PM MME had many fewer individual
618 forecasts when it was ranked as the least skillful model (Figure 6). This result demonstrates the
619 value of hedging through MMEs. Even when the aggregate forecast skill of the PM MME is not
620 significantly improved compared to its individual models, the process MME still provides value
621 by preventing the generation of poorly-performing forecasts that can occur from individual
622 models (Doblas-Reyes et al., 2005; Hagedorn et al., 2005).

623 Overall, the performance of the individual PMs was highly positively correlated (Figure 5),
624 limiting the amount of unique information provided by individual models to the MME. Others
625 have found that MME forecasts were most skillful when the covariance among models was low
626 (Dormann et al., 2018; Renwick et al., 2018), as well as when models exhibit diverging bias in
627 their mean predictions (Dormann et al., 2018; Petropoulos et al., 2022). This finding supports
628 the need for more diverse model structures to fully optimise the MME forecasts. In this study,
629 high covariance among PMs was likely caused by three key drivers. First, the three process
630 models were all 1-D hydrodynamic models. Examining whether adding more complex process
631 models (e.g., 3-D models) or simpler process models (e.g., Hanson et al., 2023) could help
632 reduce inter-model covariance is another opportunity for further research. Second, the three
633 PMs all used the same forecasted weather from the NOAA Global Ensemble Forecasting
634 System as driver data. Future work could include models that use alternative weather drivers,
635 such as different weather forecast products (e.g. Buizza & Richardson, 2017) or historical
636 weather climatology. Third, all three PMs applied the same data assimilation algorithm (an
637 ensemble Kalman filter). Future work could explore the influence of the diversity of data
638 assimilation algorithms on MME forecasts by including alternative data assimilation approaches,
639 such as a particle filter (Fearnhead & Künsch, 2018).

640 4.3 Including baseline models in the MME improved forecast skill

641 Results from the full MME demonstrate that more model diversity within an MME increases
642 forecast skill (Figure 4c; Table 1). The most model diversity was added to the MME by including
643 the two baseline models that represent end members of empirical models. Specifically, the
644 persistence model represents the most recent data and climatology represents the long-term
645 historical average for the forecasted system. By including these baseline empirical models,
646 water temperature forecast performance was substantially increased compared to the PM MME
647 (Table 1).

648 Including baseline models in an MME presents a relatively easy approach with low
649 computational costs to improve forecast performance if data are readily available for
650 constructing the baseline models. While many forecasting studies use baseline models as null
651 models to evaluate forecasts, here we show their value as a component of the forecast
652 themselves. These baseline models, despite their simplicity, provide additional forecast
653 information that the complex process models do not, and highlight that model complexity does
654 not necessarily translate to forecast skill (Viboud et al., 2018; Ward et al., 2014). Even simple
655 models, lacking any domain expertise, can provide useful information to an MME (Wang et al.,
656 2022). For example, forecasting of penguin populations showed that simpler domain-agnostic
657 time series models produced better forecasts than complex domain-specific population models
658 (Humphries et al., 2018).

659 4.4 Recommendations and next steps

660 Identifying a set of models with low covariance is likely to increase aggregated forecast skill
661 from an MME relative to its individual models. In advance of producing an MME forecast, a
662 model selection process would help ensure that the MME will improve skill relative to individual
663 models, based on among-model covariance and individual model variance and bias (Dormann
664 et al., 2018; Hagedorn et al., 2005). It is likely that the optimal set of models to include in the
665 MME will be specific to individual sites, given how individual models perform differently among
666 lakes (e.g., Bruce et al., 2018). For example, the same forecast model performed better at some
667 lakes than others in a multi-site comparison (Thomas et al., 2023), with similar differences in
668 model performance found among sites when forecasting phytoplankton (Page et al., 2018;
669 Rousso et al., 2020).

670 Further ways to improve forecast skill should also focus on constraining uncertainty. The full
671 MME had the highest variance of any of the forecast models, which undermines some of the
672 improvement in bias from the model averaging and leaves a forecast that is likely
673 underconfident (Wang et al., 2022). Methods such as boosting, dimensionality reduction, and
674 trimming can optimise bias-variance trade-offs (Wang et al., 2022). For example, trimming the
675 tails (exterior) of the individual forecast distributions has been shown to increase confidence in
676 the MME by reducing the variance of the individual model forecasts before being combined into
677 an MME (Howerton et al., 2023; Zhao et al., 2022). Previous results showed that MMEs were
678 more successful when their component model forecasts were overconfident (low variance)
679 (Hagedorn et al., 2005; Wang et al., 2022; Weigel et al., 2008).

680 Finally, our results demonstrate the value of calculating multiple evaluation metrics when
681 assessing the skill of forecasting methods, as each metric highlights potential areas to improve
682 overall skill. For example, the forecast standard deviation evaluation showed that uncertainty
683 was much larger for the MMEs than any individual model (Figure 7c, d). Simultaneously, the
684 MMEs had the lowest bias (Figure 7a, b). The IGN score was able to combine these two
685 evaluation components into a single metric of statistical performance, highlighting that
686 improvements in overall performance would likely come from reducing forecast uncertainty.
687 Although shadowing time is a metric infrequently used in freshwater forecast evaluation (Lofton
688 et al., 2023), it is potentially valuable, given its focus on the model's ability to replicate actual
689 dynamics, rather than just the statistics of the forecast (Gilmour & Smith, 1997; Petropoulos et
690 al., 2022) or the shape of the distribution (Smith et al., 2015), providing information on likely lead
691 times at which a forecast will have utility (Smith et al., 2010). Improving the capacity of the PMs
692 to have longer shadowing times may help improve their overall representation of lake and
693 reservoir dynamics.

694 **5 Conclusions**

695 This work has demonstrated the usefulness of multi-model ensembles in improving water
696 temperature forecasts. A five-model MME had the highest forecast skill among all of the
697 forecasts generated by individual models or a three-model MME, which is likely due to hedging:
698 the five-model MME was able to avoid generating very bad forecasts despite being unable to
699 provide the most skillful forecast at many individual horizons or depths. The addition of two
700 baseline models, which had low covariance with the PM models, into the MME provided useful

701 shadowing ability and complementary forecast information. Our results present an example of
702 how existing models can be combined to improve water temperature forecasting in lakes and
703 reservoirs. Future work could focus on including additional forecasting model structures to
704 further increase the diversity of predictions included in the MME and investigate optimal
705 methods to blend predictions and constrain model variance. Altogether, we highlight the value of
706 including simple baseline models (which may in some cases be already calculated as null
707 models for forecast evaluation) into multi-model ensembles for forecasting to improve
708 forecasting skill effectively and efficiently with little additional effort.

709 **Acknowledgments**

710 This work was supported by US National Science Foundation grants DEB-1926388, DBI-
711 1933016, DBI-1933102, and DEB-2320730.

712 **Data Availability Statement**

713 All data and code to produce the forecasts, scores, and figures presented in this manuscript are
714 available in in the Zenodo repositories (Olsson et al., 2023a, 2023b) or the Environmental Data
715 Initiative repositories (Carey et al., 2023; Carey & Breef-Pilz, 2023).

716 **Author contribution statement**

717 RQT and CCC developed the FLARE forecasting framework. RQT and TNM developed the
718 FLARE-LER methodology and adapted the lake models for the FLARE framework. FO led the
719 baseline model forecast generation, ran the forecasts, updated individual process-model
720 parameterization, developed the forecast evaluation framework, and analysed the forecasts with
721 RQT. ABP oversaw sensor data collection and field sampling. FO led manuscript writing with
722 RQT and CCC; all authors reviewed and approved the final version.

723

724

725 **References**

- 726 Abraham, R. J., & See, L. (2002). Multi-model data fusion for river flow forecasting: An
727 evaluation of six alternative methods based on two contrasting catchments. *Hydrology and*
728 *Earth System Sciences*, 6(4), 655–670. <https://doi.org/10.5194/hess-6-655-2002>
- 729 Almeida, M. C., Shevchuk, Y., Kirillin, G., Soares, P. M., Cardoso, R. M. A. de P., Matos, J. P.,
730 et al. (2022). Modeling reservoir surface temperatures for regional and global climate
731 models: a multi-model study on the inflow and level variation effects. *Geoscientific Model*
732 *Development*, (15), 137–197. <https://doi.org/10.5194/gmd-2021-64>
- 733 Atiya, A. F. (2020). Why does forecast combination work so well? *International Journal of*
734 *Forecasting*, 36(1), 197–200. <https://doi.org/10.1016/j.ijforecast.2019.03.010>
- 735 Baracchini, T., Wüest, A., & Bouffard, D. (2020). Meteolakes: An operational online three-
736 dimensional forecasting platform for lake hydrodynamics. *Water Research*, 172, 115529.
737 <https://doi.org/10.1016/j.watres.2020.115529>
- 738 Barrow, D. K., & Kourentzes, N. (2016). Distributions of forecasting errors of forecast
739 combinations: Implications for inventory management. *International Journal of Production*
740 *Economics*, 177, 24–33. <https://doi.org/10.1016/j.ijpe.2016.03.017>
- 741 Boettiger, C. (2022). The forecast trap. *Ecology Letters*, 25(7), 1655–1664.
742 <https://doi.org/10.1111/ele.14024>
- 743 Bradford, J. B., Weltzin, J. F., McCormick, M., Baron, J., Bowen, Z., Bristol, S., et al. (2020).
744 *Ecological Forecasting—21st Century Science for 21st Century Management. U.S.*
745 *Geological Survey Open-File Report 2020-1073.*
746 <https://doi.org/https://doi.org/10.3133/ofr20201073>
- 747 Bruce, L. C., Frassl, M. A., Arhonditsis, G. B., Gal, G., Hamilton, D. P., Hanson, P. C., et al.
748 (2018). A multi-lake comparative analysis of the General Lake Model (GLM): Stress-testing
749 across a global observatory network. *Environmental Modelling & Software*, 102, 274–291.
750 <https://doi.org/10.1016/J.ENVSOFT.2017.11.016>
- 751 Buizza, R., & Richardson, D. (2017). 25 Years of ensemble prediction. *ECMWF Newsletter*,
752 153, 20–31. <https://doi.org/10.21957/bv418o>

- 753 Carey, C. C., & Breef-Pilz, A. (2023). Ice cover data for Falling Creek Reservoir and Beaverdam
754 Reservoir, Vinton, Virginia, USA for 2013-2023 ver. 1. Environmental Data Initiative.
755 Retrieved from [https://portal-](https://portal-s.edirepository.org/nis/mapbrowse?scope=edi&identifier=1076&revision=1)
756 [s.edirepository.org/nis/mapbrowse?scope=edi&identifier=1076&revision=1](https://portal-s.edirepository.org/nis/mapbrowse?scope=edi&identifier=1076&revision=1)
- 757 Carey, C. C., Ibelings, B. W., Hoffmann, E. P., Hamilton, D. P., & Brookes, J. D. (2012). Eco-
758 physiological adaptations that favour freshwater cyanobacteria in a changing climate.
759 *Water Research*, 46(5), 1394–1407. <https://doi.org/10.1016/j.watres.2011.12.016>
- 760 Carey, C. C., Woelmer, W. M., Lofton, M. E., Figueiredo, R. J., Bookout, B. J., Corrigan, R. S.,
761 et al. (2022). Advancing lake and reservoir water quality management with near-term,
762 iterative ecological forecasting. *Inland Waters*, 12(1), 107–120.
763 <https://doi.org/10.1080/20442041.2020.1816421>
- 764 Carey, C. C., Lewis, A. S. L., Howard, D. W., Woelmer, W. M., Gantzer, P. A., Bierlein, K. A., et
765 al. (2022). Bathymetry and watershed area for Falling Creek Reservoir, Beaverdam
766 Reservoir, and Carvins Cove Reservoir. Environmental Data Initiative.
767 <https://doi.org/https://doi.org/10.6073/pasta/352735344150f7e77d2bc18b69a22412>
- 768 Carey, C. C., Breef-Pilz, A., & Woelmer, W. M. (2023). Time series of high-frequency sensor
769 data measuring water temperature, dissolved oxygen, pressure, conductivity, specific
770 conductance, total dissolved solids, chlorophyll a, phycocyanin, fluorescent dissolved
771 organic matter, and turbidity at discrete dept. Environmental Data Initiative.
772 <https://doi.org/https://doi.org/10.6073/pasta/f6bb4f5f602060dec6652ff8eb555082>
- 773 Chandler, R. E. (2013). Exploiting strength, discounting weakness: combining information from
774 multiple climate simulators. *Philosophical Transactions of the Royal Society A:*
775 *Mathematical, Physical and Engineering Sciences*, 371(1991), 20120388.
776 <https://doi.org/10.1098/rsta.2012.0388>
- 777 Clark, N. J., Proboste, T., Weerasinghe, G., & Magalhães, R. J. S. (2022). Near-term
778 forecasting of companion animal tick paralysis incidence: An iterative ensemble model.
779 *PLoS Computational Biology*, 18(2), e1009874.
780 <https://doi.org/10.1371/journal.pcbi.1009874>
- 781 Clayer, F., Jackson-Blake, L., Mercado-Bettín, D., Shikhani, M., French, A., Moore, T., et al.

- 782 (2023). Sources of skill in lake temperature, discharge and ice-off seasonal forecasting
783 tools. *Hydrology and Earth System Sciences*, 27(6), 1361–1381.
784 <https://doi.org/10.5194/hess-27-1361-2023>
- 785 Daneshmand, V., Breef-Pilz, A., Carey, C. C., Jin, Y., Ku, Y. J., Subratie, K. C., et al. (2021).
786 Edge-to-cloud virtualized cyberinfrastructure for near real-time water quality forecasting in
787 lakes and reservoirs. *Proceedings - IEEE 17th International Conference on ESience*,
788 *EScience 2021*, 138–148. <https://doi.org/10.1109/ESCIENCE51609.2021.00024>
- 789 Dietze, M. C., Fox, A., Beck-Johnson, L. M., Betancourt, J. L., Hooten, M. B., Jarnevich, C. S.,
790 et al. (2018). Iterative near-term ecological forecasting: Needs, opportunities, and
791 challenges. *Proceedings of the National Academy of Sciences*, 115(7), 1424–1432.
792 <https://doi.org/10.1073/pnas.1710231115>
- 793 Doblus-Reyes, F. J., Hagedorn, R., & Palmer, T. N. (2005). The rationale behind the success of
794 multi-model ensembles in seasonal forecasting – II. Calibration and combination. *Tellus A:*
795 *Dynamic Meteorology and Oceanography*, 57(3), 234–252.
796 <https://doi.org/10.3402/tellusa.v57i3.14658>
- 797 Dormann, C. F., Calabrese, J. M., Guillera-Arroita, G., Matechou, E., Bahn, V., Bartoń, K., et al.
798 (2018). Model averaging in ecology: a review of Bayesian, information-theoretic, and
799 tactical approaches for predictive inference. *Ecological Monographs*, 88(4), 485–504.
800 <https://doi.org/10.1002/ecm.1309>
- 801 Evensen, G. (2003). The Ensemble Kalman Filter: theoretical formulation and practical
802 implementation. *Ocean Dynamics*, 53(4), 343–367. [https://doi.org/10.1007/s10236-003-](https://doi.org/10.1007/s10236-003-0036-9)
803 [0036-9](https://doi.org/10.1007/s10236-003-0036-9)
- 804 Fearnhead, P., & Künsch, H. R. (2018). Particle filters and data assimilation. *Annual Review of*
805 *Statistics and Its Application*, 5, 421–449. [https://doi.org/10.1146/annurev-statistics-](https://doi.org/10.1146/annurev-statistics-031017-100232)
806 [031017-100232](https://doi.org/10.1146/annurev-statistics-031017-100232)
- 807 Feldbauer, J., Ladwig, R., Mesman, J. P., Moore, T. N., Zündorf, H., Berendonk, T. U., &
808 Petzoldt, T. (2022). Ensemble of models shows coherent response of a reservoir’s
809 stratification and ice cover to climate warming. *Aquatic Sciences*, 84, 50.
810 <https://doi.org/10.1007/s00027-022-00883-2>

- 811 La Fuente, S., Jennings, E., Gal, G., Kirillin, G., Shatwell, T., Ladwig, R., et al. (2022). Multi-
812 model projections of future evaporation in a sub-tropical lake. *Journal of Hydrology*, 615,
813 128729. <https://doi.org/10.1016/j.jhydrol.2022.128729>
- 814 Gilmour, I., & Smith, L. A. (1997). Enlightenment in shadows. In *Nonlinear Dynamics and*
815 *Stochastic Systems Near the Millenium* (pp. 335–340). AIP. [https://doi.org/1-56396-736-](https://doi.org/1-56396-736-7/97/)
816 *7/97/*
- 817 Golub, M., Thiery, W., Marcé, R., Pierson, D., Vanderkelen, I., Mercado-Bettin, D., et al. (2022).
818 A framework for ensemble modelling of climate change impacts on lakes worldwide: the
819 ISIMIP Lake Sector. *Geoscientific Model Development*, 15(11), 4597–4623.
820 <https://doi.org/10.5194/gmd-15-4597-2022>
- 821 Good, I. J. (1952). Rational decisions. *Journal of the Royal Statistical Society: Series B*
822 *(Methodological)*, 14(1), 107–114.
- 823 Goudsmit, G.-H., Burchard, H., Peeters, F., & Wüest, A. (2002). Application of k- ϵ turbulence
824 models to enclosed basins: The role of internal seiches. *Journal of Geophysical Research:*
825 *Oceans*, 107(C12), 3230. <https://doi.org/10.1029/2001JC000954>
- 826 Graf, R., Zhu, S., & Sivakumar, B. (2019). Forecasting river water temperature time series using
827 a wavelet–neural network hybrid modelling approach. *Journal of Hydrology*, 578, 124115.
828 <https://doi.org/10.1016/j.jhydrol.2019.124115>
- 829 Hagedorn, R., Doblas-Reyes, F. J., & Palmer, T. N. (2005). The rationale behind the success of
830 multi-model ensembles in seasonal forecasting – I. Basic concept. *Tellus A: Dynamic*
831 *Meteorology and Oceanography*, 57(3), 219. <https://doi.org/10.3402/tellusa.v57i3.14657>
- 832 Hamill, T. M., Whitaker, J. S., Shlyaeva, A., Bates, G., Fredrick, S., Pegion, P., et al. (2022).
833 The Reanalysis for the Global Ensemble Forecast System, Version 12. *Monthly Weather*
834 *Review*, 150(1), 59–79. <https://doi.org/10.1175/MWR-D-21-0023.1>
- 835 Hanson, P. C., Ladwig, R., Buelo, C., Albright, E. A., Delany, A. D., Carey, C., et al. (2023).
836 Legacy phosphorus and ecosystem memory control future water quality in a eutrophic lake.
837 *Preprint*. <https://doi.org/10.22541/essoar.168677211.11983579/v1>
- 838 Hipsey, M. R., Bruce, L. C., Boon, C., Busch, B., Carey, C. C., Hamilton, D. P., et al. (2019). A

- 839 General Lake Model (GLM 3.0) for linking with high-frequency sensor data from the Global
840 Lake Ecological Observatory Network (GLEON). *Geoscientific Model Development*, 12(1),
841 473–523. <https://doi.org/10.5194/gmd-12-473-2019>
- 842 Howerton, E., Runge, M. C., Bogich, T. L., Borchering, R. K., Inamine, H., Lessler, J., et al.
843 (2023). Context-dependent representation of within- and between-model uncertainty:
844 aggregating probabilistic predictions in infectious disease epidemiology. *Journal of The*
845 *Royal Society Interface*, 20, 20220659. <https://doi.org/10.1098/rsif.2022.0659>
- 846 Huang, B., Langpap, C., & Adams, R. M. (2011). Using instream water temperature forecasts
847 for fisheries management: An application in the pacific northwest. *Journal of the American*
848 *Water Resources Association*, 47(4), 861–876. [https://doi.org/10.1111/j.1752-](https://doi.org/10.1111/j.1752-1688.2011.00562.x)
849 [1688.2011.00562.x](https://doi.org/10.1111/j.1752-1688.2011.00562.x)
- 850 Humphries, G. R. W., Che-Castaldo, C., Bull, P. J., Lipstein, G., Ravia, A., Carrión, B., et al.
851 (2018). Predicting the future is hard and other lessons from a population time series data
852 science competition. *Ecological Informatics*, 48, 1–11.
853 <https://doi.org/10.1016/j.ecoinf.2018.07.004>
- 854 Hyndman, R. J., & Athanasopoulos, G. (2021). Forecasting: principles and practice. Retrieved
855 June 28, 2023, from OTexts.com/fpp3
- 856 IPCC (Intergovernmental Panel on Climate Change). (2023). *Technical Summary. Climate*
857 *Change 2021 – The Physical Science Basis*. Cambridge University Press.
858 <https://doi.org/10.1017/9781009157896.002>
- 859 Jackson-Blake, L. A., Clayer, F., Haande, S., Sample, J. E., & Moe, S. J. (2022). Seasonal
860 forecasting of lake water quality and algal bloom risk using a continuous Gaussian
861 Bayesian network. *Hydrology and Earth System Sciences*, 26(12), 3103–3124.
862 <https://doi.org/10.5194/hess-26-3103-2022>
- 863 Johansson, M. A., Apfeldorf, K. M., Dobson, S., Devita, J., Buczak, A. L., Baugher, B., et al.
864 (2019). An open challenge to advance probabilistic forecasting for dengue epidemics.
865 *Proceedings of the National Academy of Sciences of the United States of America*,
866 116(48), 24268–24274. <https://doi.org/10.1073/pnas.1909865116>
- 867 Jolliffe, I. T., & Stephenson, D. B. (2012). *Forecast verification: a practitioner's guide in*

868 *atmospheric science*. (I. T. Jolliffe & D. B. Stephenson, Eds.) (2nd ed.). Oxford: Wiley
869 Blackwell.

870 Jordan, A., Krüger, F., & Lerch, S. (2019). Evaluating Probabilistic Forecasts with scoringRules.
871 *Journal of Statistical Software*, 90(12), 1–37. <https://doi.org/10.18637/jss.v090.i12>

872 Kirtman, B. P., Min, D., Infanti, J. M., Kinter, J. L., Paolino, D. A., Zhang, Q., et al. (2014). The
873 North American Multimodel Ensemble: Phase-1 Seasonal-to-Interannual Prediction;
874 Phase-2 toward Developing Intraseasonal Prediction. *Bulletin of the American*
875 *Meteorological Society*, 95(4), 585–601. <https://doi.org/10.1175/BAMS-D-12-00050.1>

876 Kraemer, B. M., Chandra, S., Dell, A. I., Dix, M., Kuusisto, E., Livingstone, D. M., et al. (2017).
877 Global patterns in lake ecosystem responses to warming based on the temperature
878 dependence of metabolism. *Global Change Biology*, 23(5), 1881–1890.
879 <https://doi.org/10.1111/gcb.13459>

880 Lapeyrolerie, M., & Boettiger, C. (2023). Limits to ecological forecasting: Estimating uncertainty
881 for critical transitions with deep learning. *Methods in Ecology and Evolution*, 14(3), 785–
882 798. <https://doi.org/10.1111/2041-210X.14013>

883 Lewis, A. S. L. L., Woelmer, W. M., Wander, H. L., Howard, D. W., Smith, J. W., McClure, R. P.,
884 et al. (2022). Increased adoption of best practices in ecological forecasting enables
885 comparisons of forecastability. *Ecological Applications*, 32(2), e02500.
886 <https://doi.org/10.1002/eap.2500>

887 Lofton, M. E., Howard, D. W., Thomas, R. Q., & Carey, C. C. (2023). Progress and opportunities
888 in advancing near-term forecasting of freshwater quality. *Global Change Biology*, 29(7),
889 1691–1714. <https://doi.org/10.1111/gcb.16590>

890 Long, X., Widlansky, M. J., Spillman, C. M., Kumar, A., Balmaseda, M., Thompson, P. R., et al.
891 (2021). Seasonal Forecasting Skill of Sea-Level Anomalies in a Multi-Model Prediction
892 Framework. *Journal of Geophysical Research: Oceans*, 126, e2020JC017060.
893 <https://doi.org/10.1029/2020JC017060>

894 Machete, R. L., & Smith, L. A. (2016). Demonstrating the value of larger ensembles in
895 forecasting physical systems. *Tellus A: Dynamic Meteorology and Oceanography*, 68(1),
896 28393. <https://doi.org/10.3402/tellusa.v68.28393>

- 897 Mercado-Bettín, D., Clayer, F., Shikhani, M., Moore, T. N., Frías, M. D., Jackson-Blake, L., et al.
898 (2021). Forecasting water temperature in lakes and reservoirs using seasonal climate
899 prediction. *Water Research*, 201, 117286. <https://doi.org/10.1016/j.watres.2021.117286>
- 900 Mironov, D. V. (2021). *Parameterization of Lakes in Numerical Weather Prediction Description*
901 *of a Lake Model. COSMO Technical Report*. Offenbach am Main, Germany.
902 https://doi.org/10.1007/978-3-030-58292-0_60177
- 903 Moore, T. N., Mesman, J. P., Ladwig, R., Feldbauer, J., Olsson, F., Pilla, R. M., et al. (2021).
904 LakeEnsemblR: An R package that facilitates ensemble modelling of lakes. *Environmental*
905 *Modelling & Software*, 143, 105101. <https://doi.org/10.1016/j.envsoft.2021.105101>
- 906 O'Hara-Wild, M., Hyndman, R., & Wang, E. (2022). fable: Forecasting Models for Tidy Time
907 Series. R package version 0.3.2. Retrieved from <https://cran.r-project.org/package=fable>
- 908 Olsson, F., Moore, T. N., Carey, C. C., Breef-Pilz, A., & Thomas, R. Q. (2023a). A multi-model
909 ensemble of baseline and process-based models improves the predictive skill of near-term
910 lake forecasts: data, forecasts, and scores [dataset]. Zenodo.
911 <https://doi.org/10.5281/zenodo.8136960>
- 912 Olsson, F., Moore, T., Carey, C. C., Breef-Pilz, A., & Thomas, R. Q. (2023b). OlssonF/FCRE-
913 forecast-code: A multi-model ensemble of baseline and process-based models improves
914 the predictive skill of near-term lake forecasts: code (v1.0.0). Zenodo.
915 <https://doi.org/https://doi.org/10.5281/zenodo.8172783>
- 916 Page, T., Smith, P. J., Beven, K. J., Jones, I. D., Elliott, J. A., Maberly, S. C., et al. (2018).
917 Adaptive forecasting of phytoplankton communities. *Water Research*, 134, 74–85.
918 <https://doi.org/10.1016/j.watres.2018.01.046>
- 919 Pappenberger, F., Ramos, M. H., Cloke, H. L., Wetterhall, F., Alfieri, L., Bogner, K., et al.
920 (2015). How do I know if my forecasts are better? Using benchmarks in hydrological
921 ensemble prediction. *Journal of Hydrology*, 522, 697–713.
922 <https://doi.org/10.1016/j.jhydrol.2015.01.024>
- 923 Petropoulos, F., Apiletti, D., Assimakopoulos, V., Babai, M. Z., Barrow, D. K., Ben Taieb, S., et
924 al. (2022). Forecasting: theory and practice. *International Journal of Forecasting*, 38(3),
925 705–871. <https://doi.org/10.1016/j.ijforecast.2021.11.001>

- 926 R Core Team. (2021). R: A Language and environment for statistical computing. Vienna,
927 Austria: R Foundation for Statistical Computing. Retrieved from <https://www.r-project.org>
- 928 Read, J. S., Jia, X., Willard, J., Appling, A. P., Zwart, J. A., Oliver, S. K., et al. (2019). Process-
929 Guided Deep Learning predictions of lake water temperature. *Water Resources Research*,
930 55(11), 9173–9190. <https://doi.org/10.1029/2019WR024922>
- 931 Renwick, K. M., Curtis, C., Kleinhesselink, A. R., Schlaepfer, D., Bradley, B. A., Aldridge, C. L.,
932 et al. (2018). Multi-model comparison highlights consistency in predicted effect of warming
933 on a semi-arid shrub. *Global Change Biology*, 24(1), 424–438.
934 <https://doi.org/10.1111/gcb.13900>
- 935 Rouso, B. Z., Bertone, E., Stewart, R., & Hamilton, D. P. (2020). A systematic literature review
936 of forecasting and predictive models for cyanobacteria blooms in freshwater lakes. *Water*
937 *Research*, 182, 115959. <https://doi.org/10.1016/j.watres.2020.115959>
- 938 Saloranta, T. M., & Andersen, T. (2007). MyLake—A multi-year lake simulation model code
939 suitable for uncertainty and sensitivity analysis simulations. *Ecological Modelling*, 207(1),
940 45–60. <https://doi.org/10.1016/j.ecolmodel.2007.03.018>
- 941 Smith, L. A., Cuéllar, M. C., Du, H., & Judd, K. (2010). Exploiting dynamical coherence: A
942 geometric approach to parameter estimation in nonlinear models. *Physics Letters, Section*
943 *A: General, Atomic and Solid State Physics*, 374(26), 2618–2623.
944 <https://doi.org/10.1016/j.physleta.2010.04.032>
- 945 Smith, L. A., Suckling, E. B., Thompson, E. L., Maynard, T., & Du, H. (2015). Towards improving
946 the framework for probabilistic forecast evaluation. *Climatic Change*, 132(1), 31–45.
947 <https://doi.org/10.1007/s10584-015-1430-2>
- 948 Spence, M. A., Blanchard, J. L., Rossberg, A. G., Heath, M. R., Heymans, J. J., Mackinson, S.,
949 et al. (2018). A general framework for combining ecosystem models. *Fish and Fisheries*,
950 19(6), 1031–1042. <https://doi.org/10.1111/faf.12310>
- 951 Thomas, R. Q., Figueiredo, R. J., Daneshmand, V., Bookout, B. J., Puckett, L. K., & Carey, C.
952 C. (2020). A Near-Term Iterative Forecasting System Successfully Predicts Reservoir
953 Hydrodynamics and Partitions Uncertainty in Real Time. *Water Resources Research*, 56,
954 e2019WR026138. <https://doi.org/10.1029/2019WR026138>

- 955 Thomas, R. Q., McClure, R. P., Moore, T. N., Woelmer, W. M., Boettiger, C., Figueiredo, R. J.,
956 et al. (2023). Near-term forecasts of NEON lakes reveal gradients of environmental
957 predictability across the US. *Frontiers in Ecology and the Environment*, 21(5), 220–226.
958 <https://doi.org/10.1002/fee.2623>
- 959 Umlauf, L., Burchard, H., & Bolding, K. (2005). GOTM - Sourcecode and Test Case
960 Documentation. Retrieved from
961 <http://www.gotm.net/pages/documentation/manual/stable/pdf/a4.pdf>
- 962 Velázquez, J. A., Anctil, F., Ramos, M. H., & Perrin, C. (2011). Can a multi-model approach
963 improve hydrological ensemble forecasting? A study on 29 French catchments using 16
964 hydrological model structures. *Advances in Geosciences*, 29, 33–42.
965 <https://doi.org/10.5194/adgeo-29-33-2011>
- 966 Viboud, C., Sun, K., Gaffey, R., Ajelli, M., Fumanelli, L., Merler, S., et al. (2018). The RAPIDD
967 ebola forecasting challenge: Synthesis and lessons learnt. *Epidemics*, 22, 13–21.
968 <https://doi.org/10.1016/j.epidem.2017.08.002>
- 969 Wander, H. L., Thomas, R. Q., Moore, T. N., Lofton, M. E., & Carey, C. (2023). Data
970 assimilation experiments inform monitoring needs for near-term ecological forecasts in a
971 eutrophic reservoir Data assimilation experiments inform monitoring needs for near-term
972 ecological forecasts in a eutrophic reservoir. *Preprint*.
973 <https://doi.org/10.22541/essoar.168500255.59108131/v1>
- 974 Wang, X., Hyndman, R. J., Li, F., & Kang, Y. (2022). Forecast combinations: An over 50-year
975 review. *International Journal of Forecasting*, 1–56.
976 <https://doi.org/10.1016/j.ijforecast.2022.11.005>
- 977 Ward, E. J., Holmes, E. E., Thorson, J. T., & Collen, B. (2014). Complexity is costly: a meta-
978 analysis of parametric and non-parametric methods for short-term population forecasting.
979 *Oikos*, 123(6), 652–661. <https://doi.org/10.1111/J.1600-0706.2014.00916.X>
- 980 Weber, M., Rinke, K., Hipsey, M. R., & Boehrer, B. (2017). Optimizing withdrawal from drinking
981 water reservoirs to reduce downstream temperature pollution and reservoir hypoxia.
982 *Journal of Environmental Management*, 197, 96–105.
983 <https://doi.org/10.1016/j.jenvman.2017.03.020>

- 984 Weigel, A. P., Liniger, M. A., & Appenzeller, C. (2008). Can multi-model combination really
985 enhance the prediction skill of probabilistic ensemble forecasts? *Quarterly Journal of the*
986 *Royal Meteorological Society*, (134), 241–260. <https://doi.org/10.1002/qj>
- 987 Wilson, H. L., Ayala, A. I., Jones, I. D., Rolston, A., Pierson, D., de Eyto, E., et al. (2020).
988 Variability in epilimnion depth estimations in lakes. *Hydrology and Earth System Sciences*,
989 *24*(11), 5559–5577. <https://doi.org/10.5194/hess-24-5559-2020>
- 990 Wynne, J. H., Woelmer, W., Moore, T. N., Thomas, R. Q., Weathers, K. C., & Carey, C. C.
991 (2023). Uncertainty in projections of future lake thermal dynamics is differentially driven by
992 lake and global climate models. *PeerJ*, *11*, e15445. <https://doi.org/10.7717/peerj.15445>
- 993 Yvon-Durocher, G., Allen, A. P., Cellamare, M., Dossena, M., Gaston, K. J., Leitao, M., et al.
994 (2015). Five Years of Experimental Warming Increases the Biodiversity and Productivity of
995 Phytoplankton. *PLOS Biology*, *13*(12), e1002324.
996 <https://doi.org/10.1371/journal.pbio.1002324>
- 997 Zhao, F., Zhan, X., Xu, H., Zhu, G., Zou, W., Zhu, M., et al. (2022). New insights into
998 eutrophication management: Importance of temperature and water residence time. *Journal*
999 *of Environmental Sciences*, *111*, 229–239. <https://doi.org/10.1016/j.jes.2021.02.033>
- 1000 Zhu, S., Ptak, M., Yaseen, Z. M., Dai, J., & Sivakumar, B. (2020). Forecasting surface water
1001 temperature in lakes: A comparison of approaches. *Journal of Hydrology*, *585*, 124809.
1002 <https://doi.org/10.1016/j.jhydrol.2020.124809>
- 1003 Zwart, J. A., Oliver, S. K., Watkins, W. D., Sadler, J. M., Appling, A. P., Corson-Dosch, H. R., et
1004 al. (2023). Near-term forecasts of stream temperature using deep learning and data
1005 assimilation in support of management decisions. *JAWRA Journal of the American Water*
1006 *Resources Association*, *59*(2), 317–337. <https://doi.org/10.1111/1752-1688.13093>
- 1007